Available online at www.sciencedirect.com
ScienceDirect
International Journal of Heat and Mass Transfer 51 (2008) 1423–1430
International Journal of HEAT and MASS TRANSFER
www.elsevier.com/locate/ijhmt

Unsteady mixed convection from a rotating vertical slender cylinder in an axial flow

Param Jeet Singh [a], S. Roy [a], I. Pop [b,*]

[a] Department of Mathematics, Indian Institute of Technology Madras, Chennai 600 036, India
[b] Faculty of Mathematics, University of Cluj, R-3400 Cluj, CP 253, Romania

Received 4 July 2007
Available online 9 January 2008

Abstract

Unsteady mixed convection flow over a rotating vertical slender cylinder under the combined effects of buoyancy force and thermal diffusion with injection/suction has been studied where the slender cylinder is inline with the flow. The effect of surface curvature is also taken into account, especially for the applications such as wire and fiber drawing, where accurate predictions are desired. The governing boundary layer equations along with the boundary conditions are first converted into dimensionless form by a non-similar transformation, and then resulting system of coupled nonlinear partial differential equations is solved by an implicit finite difference scheme in combination with the quasi-linearization technique. The effects of various parameters on velocity and temperature profiles and on skin friction coefficients and heat transfer rate at the wall are reported in the present study.

1. Introduction

Mixed convection flows over cylinder shaped bodies are often encountered in many thermal engineering application such as cooling of rotating machinery, design of rotating heat exchanger, drying of paper etc. In particular, for the multi-spinning process consists of extruding a molten polymer from an array of holes in a spinneret, the yarns that are created are cooled down by their motion in the air and by a lateral quenching air flux, while their diameter decreases because of the stretching provided by the rotating bobbin, until they solidify. The system to be studied in the present investigation, shown schematically in Fig. 1, is a rotating vertical slender cylinder in a viscous fluid when the axis of the slender cylinder is inline with the flow. Flow over cylinder considered as two dimensional as the cylinder radius is large compared to the boundary layer thickness and if the cylinder radius is of the order of the boundary layer thickness then the flow is considered as axi-symmetric. The radius of the slender cylinder is same as the order of the boundary layer thickness. Therefore, the flow considered as axi-symmetric instead of two dimensional. In the axi-symmetric flow, the governing equations contain the transverse curvature term which influences the velocity and temperature fields. The impact of transverse curvature is important in several applications such as wire and fibre drawing where accurate prediction is required and thick boundary layer can exist on slender or near slender bodies.

Slender cylinder problem for a prescribed wall temperature (PWT) case is first studied by Chen and Mucoglu [1]. Further, among many investigators, notable contribution on mixed convection flows over a vertical slender cylinder was made by Heckel et al. [2] for the case of variable surface temperature. Later, Takhar et al. [3] studied the combined heat and mass transfer along a vertical moving cylinder with a free stream velocity. Recently, Kumari and Nath [4] analyzed the effects of localized cooling/heating and suction/injection on the mixed convection flow on a thin vertical cylinder. All the above studies pertain to steady mixed convection flows over a slender cylinder. Recently, Roy and Anilkumar [5] solved unsteady mixed convection from a moving vertical slender cylinder.

* Corresponding author. Fax: +91 044 2257 4602.
E-mail address: pop.ioan@yahoo.co.uk (I. Pop).

0017-9310/$ - see front matter © 2007 Elsevier Ltd. All rights reserved.
doi:10.1016/j.ijheatmasstransfer.2007.11.024

Nomenclature

Roman letters

A	surface mass transfer parameter
C_{fx}	local skin friction coefficient in x-direction
$C_{f\theta}$	local skin friction coefficient in θ direction
f	dimensionless stream function
g	dimensionless temperature
g^*	acceleration due to gravity
Gr_x	Grashoff number
k	thermal conductivity
Nu	local Nusselt number.
Pr	Prandtl number
r_0	radius of cylinder
r	radial coordinate
$R(t^*)$	unsteady function of t^*
Re	reference Reynolds number
Re_x	Reynolds number
s	non-dimensional rotational velocity
t, t^*	dimensional and dimensionless time, respectively
T	temperature
u	axial velocity component
v	radial velocity component
x	axial coordinate

Greek symbols

α	thermal diffusivity
η	similarity variable
θ	rotational direction
λ	buoyancy parameter
λ_1	rotational parameter
μ	dynamic viscosity
υ	kinematic viscosity
ξ	transverse curvature
ρ	density
ψ	dimensional stream function

Subscripts

ω, ∞	conditions at the wall and infinity, respectively
ξ, η	denote the partial derivatives w.r.t these variables, respectively.

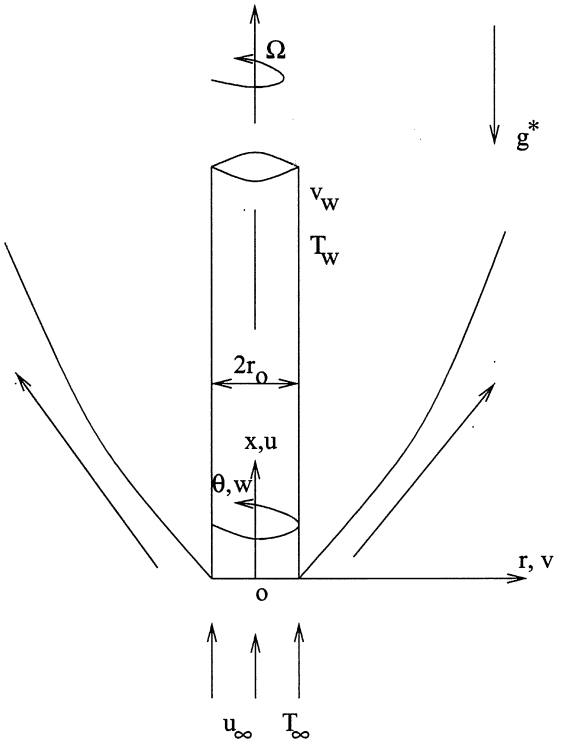

Fig. 1. Physical model and coordinate system.

In the present investigation, it is proposed to obtain the non-similar solution for the unsteady mixed convection flow over a rotating vertical slender cylinder including the effects of suction/injection, rotation and transverse curvature of the slender cylinder. The present study may have useful application to several transport processes with surface mass transfer i.e. injection (or suction) where buoyancy force arises from thermal diffusion caused by temperature gradient, such as polymer fiber coating or the coating of wires etc. In these applications, the careful control of yarn-quenching temperature or the heating and cooling temperature has a strong bearing on the final product quality [6]. The numerical results for some particular cases are matched with Chen and Mucoglu [1] and Takhar et al. [3] and found them in excellent agreement.

2. Analysis

Consider the unsteady mixed convection flow over a rotating vertical slender cylinder. The physical model and coordinate system are shown in Fig. 1. The radius of the cylinder is r_0 and the temperature of the wall and surface heat temperature vary as a function of x. The radial coordinate r is measured from the axis of the cylinder and the axial coordinate x is measured vertically upward such as $x = 0$ corresponds to the leading edge. The radius of the slender cylinder is same as the order of the boundary layer thickness. Therefore, the flow considered as axi-symmetric. Thermophysical properties of the fluid in the flow model are assumed to be constant except the density variations causing a body force term in momentum equation. The Boussinesq approximation is invoked for the fluid properties to relate density changes to temperature changes, and to couple in this way the temperature field to the flow field [7]. Under the above assumptions, the equations of conservation of mass, momentum and energy governing the mixed convection boundary layer flow over a rotating vertical slender cylinder can be expressed as

$$\frac{\partial u}{\partial x}+\frac{1}{r}\frac{\partial (rv)}{\partial r}=0, \tag{1}$$

$$\frac{\partial u}{\partial t}+u\frac{\partial u}{\partial x}+v\frac{\partial u}{\partial r}-\frac{w^2}{r}=\frac{\partial u_e}{\partial t}+\frac{v}{r}\frac{\partial}{\partial r}\left(r\frac{\partial u}{\partial r}\right)+g^*\beta(T-T_\infty) \tag{2}$$

$$\frac{\partial w}{\partial t}+u\frac{\partial w}{\partial x}+v\frac{\partial w}{\partial r}+\frac{uw}{r}=\frac{v}{r}\frac{\partial}{\partial r}\left(r\frac{\partial w}{\partial r}\right), \tag{3}$$

$$\frac{\partial T}{\partial t}+u\frac{\partial T}{\partial x}+v\frac{\partial T}{\partial r}=\frac{\alpha}{r}\frac{\partial}{\partial r}\left(r\frac{\partial T}{\partial r}\right). \tag{4}$$

The initial conditions are

$$\begin{aligned}&u(0,x,r)=u_i(x,r),\quad v(0,x,r)=v_i(x,r),\\&w(0,x,r)=w_i(x,r),\quad T(0,x,r)=T_i(x,r),\end{aligned} \tag{5}$$

and the boundary conditions are given by

$$\begin{aligned}&u(t,x,r_0)=0,\quad v(t,x,r_0)=v_w,\quad w(t,x,r_0)=\Omega r_0,\\&T(t,x,r_0)=T_w(x),\\&u(t,x,\infty)=u_e=u_\infty R(t^*),\quad w(t,x,\infty)=0,\quad T(t,x,\infty)=T_\infty.\end{aligned} \tag{6}$$

Applying the following transformations:

$$\begin{aligned}&\xi=\left(\frac{4}{r_0}\right)\left(\frac{vx}{u_\infty}\right)^{\frac{1}{2}},\quad \eta=\left(\frac{vx}{u_\infty}\right)^{-\frac{1}{2}}\left[\frac{r^2-r_0^2}{4r_0}\right],\quad t^*=\frac{tv}{r_0^2}\\&\frac{r^2}{r_0^2}=[1+\xi\eta],s=\frac{w}{r_0\Omega},\quad u=\frac{1}{r}\frac{\partial\psi}{\partial r},\quad v=-\frac{1}{r}\frac{\partial\psi}{\partial x},\\&\lambda_1=\left(\frac{r_0\Omega}{u_\infty}\right)^2,\quad \psi(t,x,r)=r_0(vu_\infty x)^{\frac{1}{2}}R(t^*)f(t^*,\xi,\eta),\\&g(t^*,\xi,\eta)=\frac{T-T_\infty}{T_w(x)-T_\infty},\quad (T_w(x)-T_\infty)=(T_{w0}-T_\infty)\frac{r_0}{x},\\&u=\frac{1}{2}u_\infty R(t^*)f_\eta(t^*,\xi,\eta),\quad v=\frac{r_0}{2r}R(t^*)\left(\frac{vu_\infty}{x}\right)^{\frac{1}{2}}(\eta f_\eta-f-\xi f_\xi),\\&Pr=\frac{v}{\alpha},\quad Re=\frac{u_\infty r_0}{v},\quad Re_x=\frac{u_\infty x}{v},\\&Gr_x=\frac{g^*\beta x^3(T_w(x)-T_\infty)}{v^2},\quad \lambda=\frac{Gr_x}{Re_x^2}\end{aligned} \tag{7}$$

to Eqs. (1)–(4), we find that Eq. (1) is satisfied identically, and Eqs. (2)–(4) reduce to

$$\begin{aligned}&(1+\xi\eta)f_{\eta\eta\eta}+(\xi+R(t^*)f)f_{\eta\eta}+8R^{-1}(t^*)\lambda g\\&\quad+\frac{\xi^2\lambda_1 Re\ s^2}{2(1+\xi\eta)^{1/2}R(t^*)}+\left(\frac{\xi^2}{4}\right)\left[R^{-1}R_{t^*}(2-f_\eta)-\frac{\partial f_\eta}{\partial t^*}\right]\\&\quad=\xi R(t^*)\left(f_\eta\frac{\partial f_\eta}{\partial\xi}-f_{\eta\eta}\frac{\partial f}{\partial\xi}\right),\end{aligned} \tag{8}$$

$$\begin{aligned}&(1+\xi\eta)s_{\eta\eta}+(\xi+R(t^*)f)s_\eta-\frac{R(t^*)\xi^2Re}{8(1+\xi\eta)^{1/2}}f_\eta s-\left(\frac{\xi^2}{4}\right)\frac{\partial s}{\partial t^*}\\&\quad=\xi R(t^*)\left(f_\eta\frac{\partial s}{\partial\xi}-s_\eta\frac{\partial f}{\partial\xi}\right),\end{aligned} \tag{9}$$

$$\begin{aligned}&Pr^{-1}(1+\xi\eta)g_{\eta\eta}+(\xi Pr^{-1}+R(t^*)f)g_n-\left(\frac{\xi^2}{4}\right)\frac{\partial g}{\partial t^*}-2R(t^*)f_\eta g\\&\quad=\xi R(t^*)\left(f_\eta\frac{\partial g}{\partial\xi}-g_\eta\frac{\partial f}{\partial\xi}\right).\end{aligned} \tag{10}$$

The boundary conditions reduce to

$$\begin{aligned}&f_n(t^*,\xi,0)=0,\quad s(t^*,\xi,0)=1,\quad g(t^*,\xi,0)=1,\ \text{at}\ \eta=0,\\&f_n(t^*,\xi,\eta_\infty)=2,\quad s(t^*,\xi,\eta_\infty)=0,\\&g(t^*,\xi,\eta_\infty)=0,\ \text{at}\ \eta=\eta_\infty,\end{aligned} \tag{11}$$

where η_∞ is the edge of the boundary layer and

$$f(t^*,\xi,0)=-\frac{r_0v_\omega\xi}{4vR(t^*)}=\frac{A\xi}{R(t^*)},\quad A=-\frac{r_0v_\omega}{4v}$$

The local skin friction coefficient in x-direction is given by

$$\begin{aligned}&C_{fx}=\frac{2[\mu\frac{\partial u}{\partial r}]_{r=r_0}}{\rho u_\infty^2}=\frac{(Re_x)^{-\frac{1}{2}}f_{\eta\eta}(t^*,\xi,0)R(t^*)}{2}\\&\text{i.e.,}\ Re_x^{\frac{1}{2}}C_{fx}=\frac{f_{\eta\eta}(t^*,\xi,0)R(t^*)}{2}.\end{aligned} \tag{12}$$

The local skin friction coefficient in θ-direction due to the rotational component of the velocity is given by

$$\begin{aligned}&C_{f\theta}=\frac{2[\mu\frac{\partial\omega}{\partial r}]_{r=r_0}}{\rho u_\infty^2}=-(Re_x)^{-\frac{1}{2}}\lambda_1^{1/2}s_\eta(t^*,\xi,0)R(t^*)\\&\text{i.e.,}\ Re_x^{\frac{1}{2}}C_{f\theta}=-\lambda_1^{1/2}s_\eta(t^*,\xi,0)R(t^*).\end{aligned} \tag{13}$$

The local heat transfer rate at the wall in terms of Nusselt number can be expressed as

$$Re_x^{-\frac{1}{2}}Nu=-2^{-1}g_\eta(t^*,\xi,0), \tag{14}$$

where $Nu=-\frac{[x(\frac{\partial T}{\partial r})]_{r=r_0}}{T_\omega-T_\infty}$.

The surface mass transfer parameter $A>0$ or $A<0$ according to whether there is suction/injection. It is assumed that the flow is unsteady due to the time dependent free stream velocity $[u_e(t)=u_\infty R(t^*)]$ where $R(t^*)=1+\alpha t^{*2}$; $\alpha>0$ or <0. Hence, the initial conditions are given by steady-state equations obtained from Eqs. (8)–(10) by substituting $R(t^*)=1,\frac{\partial R}{\partial t^*}=\frac{\partial f_\eta}{\partial t^*}=\frac{\partial s}{\partial t^*}=\frac{\partial g}{\partial t^*}=0$, when $t^*=0$. The corresponding boundary conditions are obtained from Eq. (11) at $t^*=0$.

3. Results and discussion

The non-linear coupled partial differential equations (8)–(10) under the boundary conditions given by Eq. (11) have been solved numerically using an implicit finite difference scheme in combination with the quasi-linearization technique [8]. Since the method is described in a recent study by Roy and Saikrishnan [9], it's detailed description is not provided for the sake of brevity. In brief, an iterative sequence of linear equations are carefully constructed to approximate the non-linear equations (8)–(10) achieving quadratic convergence and monotonicity. At each iteration step, the sequence of linear partial differential equations

were expressed in difference form by using finite diference scheme. Thus, in each iteration step, the resulting equations were then reduced to a system of linear algebraic equations with a block tri-diagonal matrix, which is solved by Varga's algorithm [10]. To ensure the convergence of the numerical solution to the exact solution, the step sizes $\Delta\eta$, $\Delta\xi$ and Δt^* have been optimized and taken as 0.02, 0.01 and 0.01, respectively. The results presented here are independent of the step sizes at least up to the fourth decimal place. A convergence criterion based on the relative difference between the current and previous iteration value is employed. When the difference reaches 10^{-4}, the solution is assumed to have converged and the iterative process is terminated.

Computations have been carried out for various values of $Pr(0.1 \leqslant Pr \leqslant 100.0)$, $A(-2.0 \leqslant A \leqslant 2.0)$, $\lambda(0 \leqslant \lambda \leqslant 6.0)$ and $\lambda_1(0.0 \leqslant \lambda_1 \leqslant 5.0)$. The value of reference Reynolds number (Re) is taken as 10^4 for all numerical computations. The edge of the boundary layer (η_∞) has been taken between 3 and 5 depending on the values of the parameters. To verify the correctness of our methods, we have compared some of our particular results with Chen and Mucoglu [1] and Takhar et al. [3]. The results are found in excellent agreement and some of the comparisons are shown in Table 1.

The effects of buoyancy parameter (λ) and Prandtl number (Pr) on the velocity and temperature profiles (f_η, g) for the accelerating flow $[R(t^*) = 1 + \alpha t^{*2}, \alpha = 0.5]$ when $Re = 10^4$, $A = 1$ and $\lambda_1 = 0.1$ at $\xi = 0.5$ are displayed in Fig. 2. The buoyancy force (λ) shows the presence of overshoot in the velocity profiles near the wall for lower Prandtl number fluid (air, $Pr = 0.7$) but for higher Prandtl number fluid (water, $Pr = 7.0$) the velocity overshoot is not observed. The magnitude of the overshoot increases with the buoyancy parameter (λ) but decreases as the Prandtl number increases. The reason is that the buoyancy force (λ) affects more in low Prandtl number fluid (air, $Pr = 0.7$) due to the low viscosity of the fluid, which increases the velocity within the boundary layer as the assisting buoyancy force acts like a favorable pressure gradient.

Table 1
Comparison of steady-state results $(f_{\eta\eta}(\xi,0), -g_n(\xi,0))$ when rotational parameter $\lambda_1 = 0$ and $Pr = 0.7$ with those of Chen and Mucoglu [1] and Takhar et al. [3]

ξ	λ	Present results		Chen and Mucoglu [1]		Takhar et al. [3]	
		$f_{\eta\eta}(\xi,0)$	$-g_n(\xi,0)$	$f_{\eta\eta}(\xi,0)$	$-g_n(\xi,0)$	$f_{\eta\eta}(\xi,0)$	$-g_n(\xi,0)$
0	0	1.3281	0.5854	1.3282	0.5854	1.3281	0.5854
0	1	4.9665	0.8221	4.9666	0.8221	4.9663	0.8219
0	2	7.7124	0.9303	7.7126	0.9305	7.7119	0.9302
1	0	1.9168	0.8668	1.9172	0.8669	1.9167	0.8666
1	1	5.2580	1.0618	5.2584	1.0621	5.2578	1.0617
1	2	7.8870	1.1692	7.8871	1.1690	7.8863	1.1685

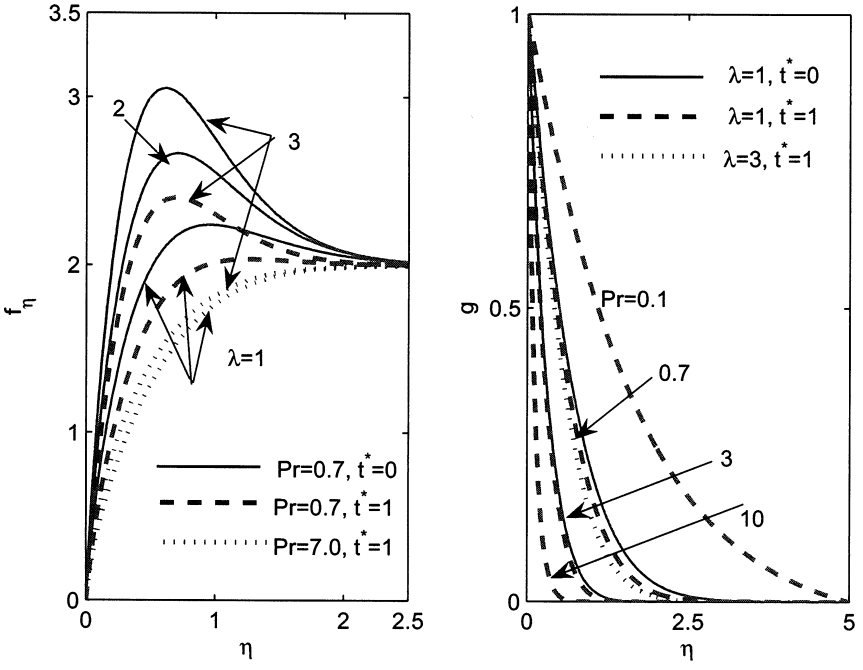

Fig. 2. Effects of λ and Pr on f_η and g for accelerating flow $[R(t^*) = 1 + \alpha t^{*2}, \alpha = 0.5]$ when $\lambda_1 = 1$, $A = 1$ and $Re = 10^4$ at $\xi = 0.5$.

Hence, the velocity overshoot occurs and for higher Prandtl number fluids the overshoot is not observed because higher Prandtl number (water, $Pr = 7.0$) implies more viscous fluid which makes it less sensitive to the buoyancy parameter (λ). The time effect is crucial for the velocity overshoot. For example, for $\alpha = 0.5$, $Re = 10^4$, $Pr = 0.7$, $A = 1$, $\lambda = 1$, $\lambda_1 = 0.1$ at $\xi = 0.5$, overshoot in the velocity (f_n) profile reduced approximately by 26% as t^* increases from 0 to 1. The effect of λ is comparatively less in temperature profile (g) as shown in Fig. 2. Moreover, Fig. 2 also shows that the effect of higher Prandtl number (Pr) results into the thinner thermal boundary layer as the higher Prandtl number fluid (water, $Pr = 7.0$) has a lower thermal conductivity.

The effects of buoyancy parameter (λ) and surface curvature parameter ξ on skin friction coefficient and surface heat transfer parameter ($C_{fx}Re_x^{1/2}, NuRe_x^{-1/2}$) are shown in Fig. 3. The skin friction coefficient and surface heat transfer parameter ($C_{fx}Re_x^{1/2}, NuRe_x^{-1/2}$) increase with the buoyancy parameter λ. The physical reason is that the positive buoyancy force ($\lambda > 0$) implies favorable pressure gradient, and the fluid gets accelerated, which result in thinner momentum and thermal boundary layers. Consequently, the local skin friction ($C_{fx}Re_x^{1/2}$) and local Nusselt number ($NuRe_x^{-1/2}$) are also increased at all times. For example, for $\alpha = 0.5$, $Re = 10^4$, $Pr = 0.7$, $A = l$, $\lambda_1 = 0.1$ and $\xi = 0$ at time $t^* = 1$, Fig. 3 shows that the percentage increase in skin friction coefficient ($C_{fx}Re_x^{1/2}$) and heat transfer parameter ($NuRe_x^{-1/2}$) are approximately 95% and 18% when λ changes from 1 to 3. Further, Fig. 3 indicates that the skin friction coefficient ($C_{fx}Re_x^{1/2}$) and heat transfer parameter ($NuRe_x^{1/2}$) increase with the increase of ξ because the increase in ξ acts as a favorable pressure gradient. Few other numerical results for various values of buoyancy parameter (λ) are tabulated in Table 2. Fig. 4 displays the effect of Prandtl number (Pr) for accelerating and decelerating free stream flows [$R(t^*) = 1 + \alpha t^{*2}$, $\alpha = 0.5$ and -0.5] on skin friction coefficients and surface heat transfer parameter ($C_{fx}Re_x^{1/2}, C_{f\theta}Re_x^{1/2}, NuRe_x^{1/2}$). In Fig. 4, skin friction coefficients ($C_{fx}Re_x^{1/2}, C_{f\theta}Re_x^{1/2}$) decrease with the increase of Prandtl number (Pr). The reason for this trend is that the higher Prandtl number fluid means more viscous fluid, which increase the boundary layer thickness and, consequently, reduce the shear stress. On the other hand, heat transfer parameter ($NuRe_x^{-1/2}$) in Fig. 4 increase significantly with the Prandtl number, as higher Prandtl number fluid has lower thermal conductivity, which results in thinner thermal boundary layer and, hence, a higher heat transfer rate at wall ($NuRe_x^{1/2}$). As a whole, it may be pointed out that the effect of Pr is more pronounced on Nusselt number

Table 2
Skin friction coefficients and heat transfer parameter ($C_{fx}Re_x^{1/2}, C_{f\theta}Re_x^{1/2}, NuRe_x^{-1/2}$) when $\xi = 0.5$, $t^* = 1$, $\lambda_1 = 1$, $\alpha = 0.5$, $Re = 10^4$ and $A = 1$

λ	Pr	$C_{fx}Re_x^{1/2}$	$C_{f\theta}Re_x^{1/2}$	$NuRe_x^{-1/2}$
1	0.1	21.6532	15.6728	0.3134
1	1	20.7849	15.2411	0.9196
1	10	20.1853	14.9211	5.1345
1	100	19.9627	14.8270	49.2816
3	0.1	24.7540	16.9040	0.3425
3	1	22.4393	15.9573	0.9666
3	10	20.6953	15.1170	5.1201
3	100	20.0168	14.8339	49.2806
6	0.1	29.1252	18.3079	0.3712
6	1	24.7798	16.8273	1.0235
6	10	21.4815	15.4092	5.1049
6	100	20.0979	14.8444	49.2792

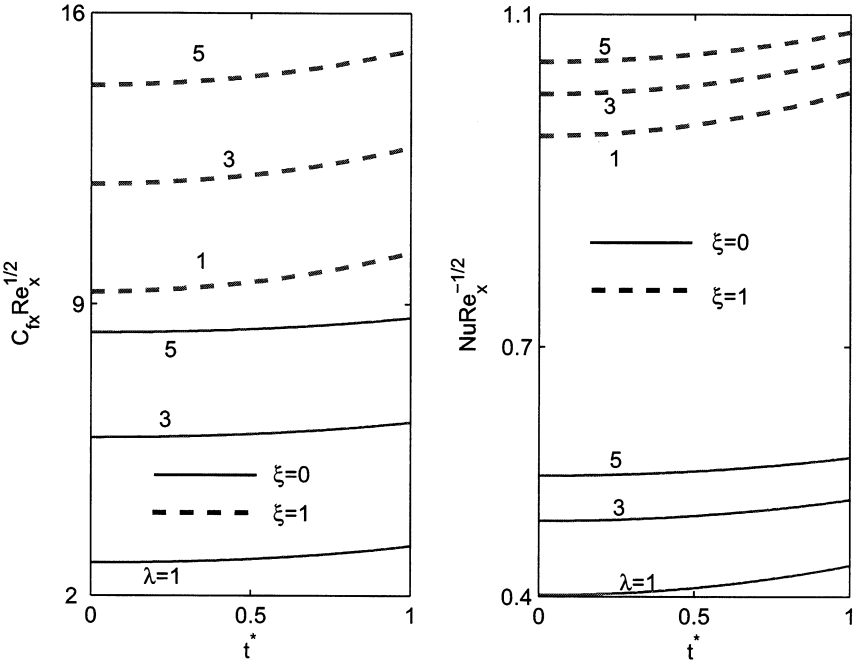

Fig. 3. Effect of λ on $C_{fx}Re_x^{1/2}$ and $NuRe_x^{1/2}$ for accelerating flow [$R(t^*) = 1 + \alpha t^{*2}$, $\alpha = 0.5$] when $\alpha_1 = 0.1$, $A = 1$, $Re = 10^4$ and $Pr = 0.7$.

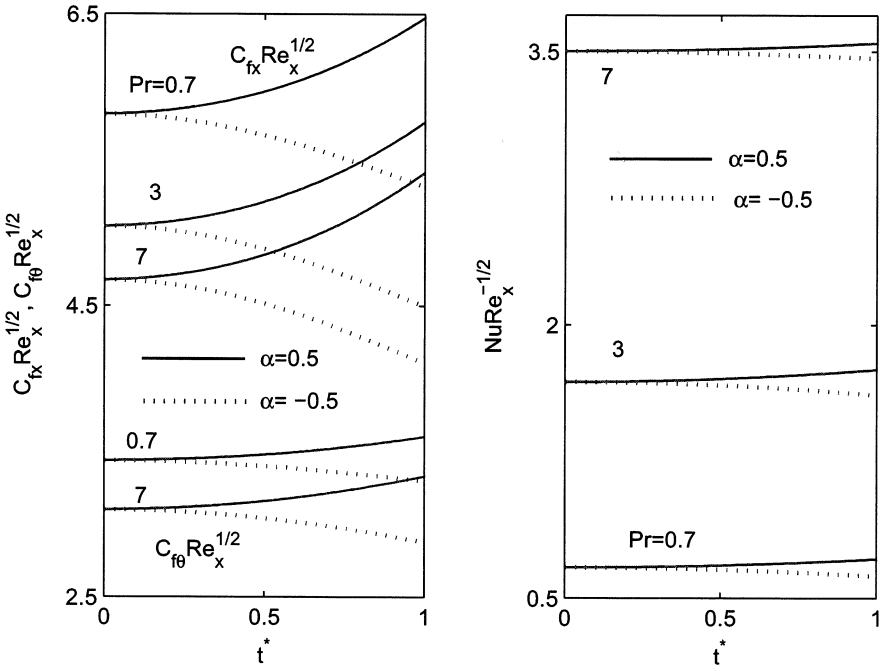

Fig. 4. Effect of Pr on $C_{fx}Re_x^{1/2}, C_{f\theta}Re_x^{1/2}$ and $NuRe_x^{-1/2}$ for accelerating and decelerating flows $[R(t^*) = 1 + \alpha t^{*2}, \alpha = 0.5$ and $-0.5]$ when $\lambda = 1$, $\lambda_1 = 0.1$, $A = 1$, $Re = 10^4$ and $Pr = 0.7$ at $\xi = 0.5$.

$(NuRe_x^{1/2})$ as compared to the skin friction coefficients $(C_{fx}Re_x^{1/2}, C_{f\theta}Re_x^{1/2})$. In particular, for $\lambda = l$, $\lambda_1 = 1$, $Re = 10^4$, $A = 1$ at $\xi = 0.5$ and $t^* = 1$, the skin friction coefficients $(C_{fx}Re_x^{1/2}, C_{f\theta}Re_x^{1/2})$ decrease by 16% and 8%, respectively and surface heat transfer parameter $(NuRe_x^{1/2})$ increases by 400% when Prandtl number varies from 0.7 to 7.0. In case of higher values of Prandtl number (Pr), some of the numerical results for skin friction coefficients and heat transfer parameter $(C_{fx}Re_x^{1/2}, C_{f\theta}Re_x^{1/2}, NuRe_x^{1/2})$ when $\xi = 0.5$, $t^* = 1$, $\lambda_1 = 1$, $\alpha = 0.5$, $Re = 10^4$ and $A = 1$ are shown in Table 2.

Fig. 5 shows the effect of rotational parameter (λ_1) on the velocity profile (f_n) and skin friction coefficients $(C_{fx}Re_x^{1/2}, C_{f\theta}Re_x^{1/2})$ When the slender cylinder rotates fas-

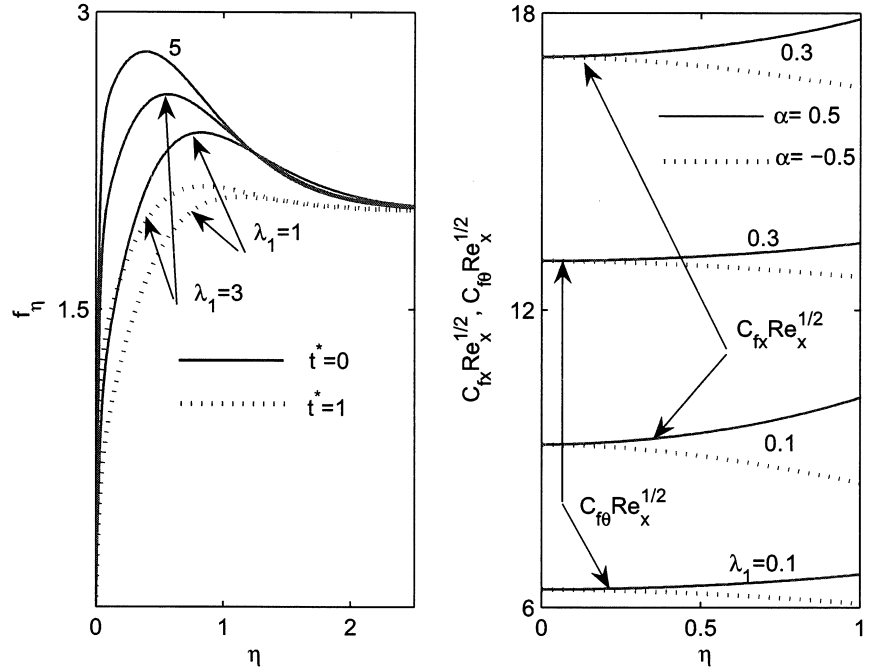

Fig. 5. (a) Effects of λ_1 on f_η for accelerating flow $[R(t^*) = 1 + \alpha t^{*2}, \alpha = 0.5]$ when $\lambda = 1$, $A = 0$, $Re = 10^4$ and $Pr = 0.7$ at $\xi = 0.5$. (b) Effect of λ_1 on $C_{fx}Re_x^{1/2}$, and $C_{f\theta}Re_x^{1/2}$ for accelerating and decelerating flows $[R(t^*) = 1 + \alpha t^{*2}, \alpha = 0.5$ and $-0.5]$ when $\lambda = 1$, $A = 1$, $Re = 10^4$ and $Pr = 0.7$ at $\xi = 1$.

ter, the velocity overshoot observed near the wall within the boundary layer because the rotating slender cylinder cause rotation in the fluid near the wall and rotating fluid with the buoyancy force moves faster near the wall compared to the fluid away from the wall. The overshoot reduces with the increase of t^*. For example, for $Pr = 0.7$, $\lambda = 1$, $\lambda_1 = 1$, $Re = 10^4$ and $\lambda = 0$ at $\xi = 0.5$, the overshoot is decreased by approximately 14% when t^* changes from 0 to 1. The skin friction coefficients ($C_{fx}Re_x^{1/2}$, $C_{f\theta}Re_x^{1/2}$) increase as the slender cylinder rotates faster i.e. as the rotation parameter increases. This is because of the fact that as the slender cylinder rotates faster, it drags more fluid near the wall and reduce the boundary layer thickness, consequently, velocity gradient increases. For example, the skin friction coefficients ($C_{fx}Re_x^{1/2}, C_{f\theta}Re_x^{1/2}$) increases approximately by 74% and 100% as λ_1 increases from 0.1

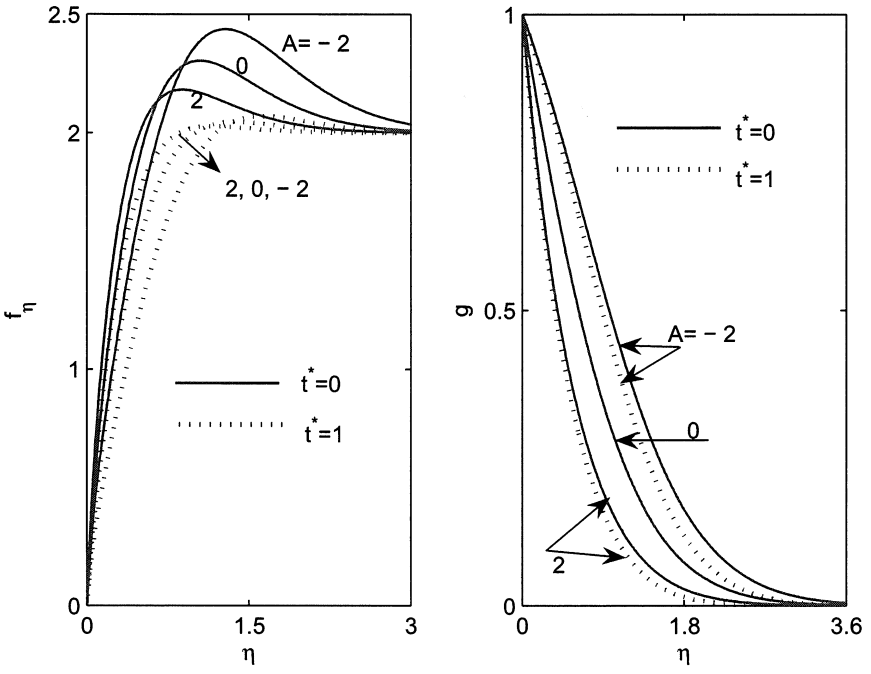

Fig. 6. Effect of A on the f_η and g for accelerating flows [$R(t^*) = 1 + \alpha t^{*2}$, $\alpha = 0.5$] when $\lambda = 1$, $\lambda_1 = 0.1$, $Re = 10^4$ and $Pr = 0.7$ at $\xi = 0.5$.

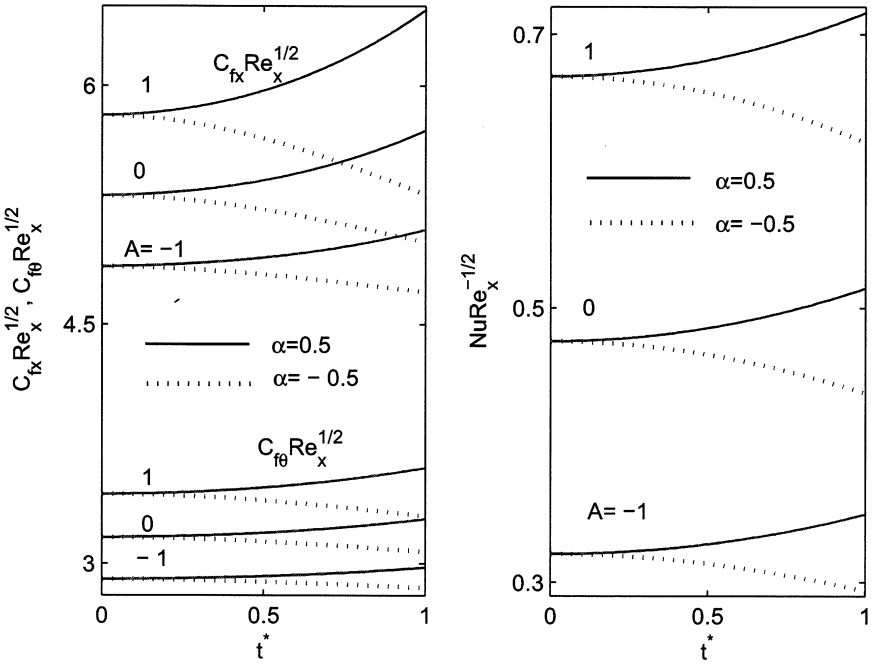

Fig. 7. Effect of A on the $C_{fx}Re_x^{1/2}$, $C_{f\theta}Re_x^{1/2}$ and $NuRe_x^{-1/2}$ for accelerating and decelerating flows [$R(t^*) = 1 + \alpha t^{*2}$, $\alpha = 0.5$ and -0.5] when $\lambda = 1$, $\lambda_1 = 0.1$, $Re = 10^4$ and $Pr = 0.7$ at $\xi = 0.5$.

to 0.3 when $\lambda = l$, $Pr = 0.7$, $Re = 10^4$, $A = 1$ at $\xi = 1$. The effect of λ_1 on the heat transfer parameter is very less and the results for Nusselt number are not presented here for the sake of brevity.

The effect of suction ($A > 0$) and injection ($A < 0$) parameter on the velocity and temperature profiles (f_η, g) are shown in Fig. 6. In case of injection, the fluid is carried away from the surface, causing reduction in the velocity gradient as it tries to maintain the same velocity over a very small region near the surface, and this effect is reversed in the case of suction. The higher velocity overshoot is observed near the wall within the boundary layer for injection ($A < 0$) and overshoot is decreased for suction ($A > 0$). Injection ($A < 0$) causes a decrease in the steepness of the velocity profile (f_η) near the wall within the boundary layer, but the steepness of the velocity profile (f_η) increases with suction. The effect of injection ($A < 0$) and suction ($A > 0$) on the skin friction and heat transfer coefficients ($C_{fx}Re_x^{1/2}, C_{f\theta}Re_x^{1/2}, NuRe_x^{-1/2}$) are shown in Fig. 7. As expected, results indicate that skin friction and heat transfer coefficients ($C_{fx}Re_x^{1/2}, C_{f\theta}Re_x^{1/2}, NuRe_x^{-1/2}$) increase with the increase of suction parameter ($A > 0$) but decrease as the magnitude of injection ($A < 0$) increase. Suction/injection parameter (A) has no effect on the skin friction coefficients and Nusselt number ($C_{fx}Re_x^{1/2}, C_{f\theta}Re_x^{1/2}, NuRe_x^{1/2}$) at $\xi = 0$ because the value of the non-dimensional stream function at the wall is equal to A multiplied by ξ i.e. $f_w = A\xi$. All the results in Fig. 7 show reverse trend for decelerating flow with the increase of t^* as compare to accelerating flow. In particular, Fig. 7 shows that the percentage increase in the skin friction coefficients and Nusselt number ($C_{fx}Re_x^{1/2}, C_{f\theta}Re_x^{1/2}, NuRe_x^{-1/2}$) are approximately 27%, 21% and 100%, respectively, for $\lambda = 1$, $Pr = 0.7$, $\lambda_1 = 0.1$ at $t^* = 1$ and $\xi = 0.5$ when A varies from -1 to 1.

4. Conclusions

Numerical results indicate that the skin friction and heat transfer coefficients are strongly affected by the time dependent free stream velocity which confirms the importance of present investigation of unsteady mixed convection flow. The buoyancy force causes overshoot in the velocity profile for low Prandtl number (Pr) fluid at $t^* = 0$ and overshoot reduces significantly as t^* increases. The surface skin friction strongly depends on the buoyancy force due to the thermal diffusion, and on the relative velocity between the wall and the free stream. Skin friction coefficients and heat transfer rate are found to alter significantly due to injection/ suction for both accelerating and decelerating free stream flows.

Acknowledgement

Authors express sincere thanks to the reviewer for the valuable suggestions and comments on our paper.

References

[1] T.S. Chen, A. Mucoglu, Buoyancy effects on forced convection along a vertical cylinder, ASME J. Heat Transfer 97 (1975) 198–203.
[2] J.J. Heckel, T.S. Chen, B.F. Armaly, Mixed convection along slender vertical cylinders with variable surface temperature, Int. J. Heat Mass Transfer 32 (1989) 1431–1442.
[3] H.S. Takhar, A.J. Chamkha, G. Nath, Combined heat and mass transfer along a vertical moving cylinder with a free stream, Heat Mass Transfer 36 (2000) 237–246.
[4] M. Kumari, G. Nath, Mixed convection boundary layer flow over a thin vertical cylinder with localised injection/suction and cooling/ heating, Int. J. Heat Mass Transfer 47 (2004) 969–976.
[5] S. Roy, D. Anilkumar, Unsteady mixed convection from a moving vertical slender cylinder, ASME J. Heat Transfer 128 (2006) 368–373.
[6] A. Ziabicki, Pundamentls of Fibre Formation, Wiley, New York, 1976.
[7] H. Schlichting, Boundary Layer Theory, Springer, New York, 2000.
[8] R.E. Bellman, R.E. Kalaba, Quasilinearization and Non-linear Boundary Value Problem, Elsevier, USA, 1965.
[9] S. Roy, P. Saikrishnan, Non-uniform slot injection (suction) into steady laminar boundary layer flow over a rotating sphere, Int. J. Heat Mass Transfer 46 (2003) 3389–3396.
[10] R.S. Varga, Matrix Iterative Analysis, Prentice Hall, 2000.